Neuroscience Research xxx (xxxx) xxx

Contents lists available at ScienceDirect

Neuroscience Research

journal homepage: www.sciencedirect.com/journal/neuroscience-research

# Postnatal development of the microstructure of cortical GABAergic synapses and perineuronal nets requires sensory input

Nikita Lipachev [a,b,1], Anastasia Melnikova [c,1], Svetlana Fedosimova [d], Nikita Arnst [c,e], Anastasia Kochneva [c], Nurislam Shaikhutdinov [c,f], Anastasia Dvoeglazova [c], Angelina Titova [c], Mikhail Mavlikeev [g], Albert Aganov [b], Yuri Osin [d], Andrei Kiyasov [c], Mikhail Paveliev [a,*]

[a] Neuroscience Center, University of Helsinki, Viikinkaari 4, P.O. Box 56, 00790 Helsinki, Finland
[b] Institute of Physics, Kazan Federal University, Kremlyovskaya 16a, 420111 Kazan, Tatarstan, Russia
[c] Institute of Fundamental Medicine and Biology, Kazan Federal University, Karl Marx 74, 420012 Kazan, Tatarstan, Russia
[d] Interdisciplinary Center for Analytic Microscopy, Kazan Federal University, Parizhskoy Kommuny 9, 420021 Kazan, Tatarstan, Russia
[e] Department of Biomedical Sciences, University of Padua, via U. Bassi 58/B, 35131 Padua, Italy
[f] Center of Life Sciences, Skolkovo Institute of Science and Technology, Moscow, Russia
[g] Department of Pathological Anatomy, North-Western State Medical University named after I.I.Mechnikov, Piskarevskiy prospect 47, Build. 23, 195067 Saint-Petersburg, Russia

ARTICLE INFO

*Keywords:*
Perineuronal nets
GABAergic synapses
Postnatal development
Quantitative analysis

ABSTRACT

The brain synaptic circuitry is formed as a result of pre-defined genetic programs and sensory experience during postnatal development. Perineuronal nets ensheath synaptic boutons and control several crucial features of the synapse physiology. Formation of the perineuronal net microstructure during the brain development remains largely unstudied. Here we provide a detailed quantitative description of the 3-dimensional geometry of the synapse and the surrounding perineuronal net in the mouse somatosensory cortex layer IV. We compare the morphology of the synapse+perineuronal net complex in the adult brain formed under normal conditions or in the whisker shaving model of somatosensory deprivation. We demonstrate that the sensory deprivation causes flattening of the 3D PNN mesh geometry and reduction of the VGAT-positive cluster volume in presynaptic boutons. These results reveal a mechanism of the sensory input-dependent synapse morphogenesis during the brain development.

## 1. Introduction

Sculpturing of synaptic networks by sensory experience is currently recognized as a fundamental mechanism of the brain plasticity (Fawcett et al., 2019; Ferrer-Ferrer and Dityatev, 2018). This phenomenon of the experience-dependent synaptic rearrangements is comprised by a number of molecular processes both in the synapses and in the surrounding extracellular matrix (Dzyubenko et al., 2016).

Perineuronal net (PNN) is a highly structured subtype of extracellular matrix surrounding synaptic boutons on neuronal cell bodies and proximal dendrites in large neuronal populations in the brain and spinal cord (Sorg et al., 2016; Miyata and Kitagawa, 2017). Starting from the pioneering work of Pizzorusso and co-authors a large body of experimental evidence accumulated showing that PNN restrict neuronal plasticity, i.e., rewiring of synaptic networks in the adult brain (Pizzorusso et al., 2002).

The PNN development takes place during the critical period of the brain maturation and is controlled by synaptic activity within the network (Carulli et al., 2010; McRae et al., 2007; Nowicka et al., 2009; Lander et al., 1997; Brückner et al., 2004). Synaptic activity-dependent changes in PNN include changes in the expression of three different CSPG epitopes (Lander et al., 1997) and aggrecan mRNA (McRae et al., 2007).

High resolution PNN microstructure remained unstudied until recently (Arnst et al., 2016). Quantitative changes have been now demonstrated at the single mesh level in experimental models of focal cerebral ischemia (Dzyubenko et al., 2018), Rett syndrome (Sigal et al., 2019) and schizophrenia (Kaushik et al., 2020).

* Corresponding author.
*E-mail address:* paveliev@outlook.com (M. Paveliev).
[1] These two authors contributed equally to the study

https://doi.org/10.1016/j.neures.2022.06.005
Received 3 February 2022; Received in revised form 4 June 2022; Accepted 9 June 2022
Available online 13 June 2022

In the present study we analyzed microstructure of the complex of GABAergic synapses with PNN in the mouse somatosensory cortex and compared its formation in the presence versus absence of sensory input during the critical period of early postnatal development. We demonstrate that the sensory input is required for the proper morphology formation of the presynaptic terminal and the surrounding PNN.

## 2. Materials and methods

### 2.1. Animals

For sensory deprivation experiments mice were subjected to whisker shaving once a day during P0-P30. Unshaved littermates were used as control.

### 2.2. Tissue preparation

Mouse brain samples were collected according to regulations of the ethics committee of Kazan Federal University. For immunohistochemistry animals were terminally anaesthetized with an intraperitoneal overdose of Urethane (Sigma-Aldrich) and were immediately perfused through the heart with 40 ml of cold phosphate- buffered saline (PBS, pH 7.4), followed by the same volume of cold 4% paraformaldehyde. Brains were removed and postfixed over- night in 4% paraformaldehyde at + 4 C. After that brains were cryoprotected with 30% sucrose in PBS, pH 7.4 for 48 h and then frozen in embedding medium (Tissue-Tek, Sakura, Japan) at − 80 °C. 18–20 micrometer-thick coronal brain sections were cut on a cryostat. The barrel cortex regions were determined using Comparative Cytoarchitectonic Atlas of Mouse Brain (Patrick R. Hof, Elsevier).

### 2.3. Staining procedure

PNN was stained with the biotinylated Wisteria floribunda Lectin (VectorLab, USA) that is generally thought to bind N-acetyl-galactosamine (GalNAc) of CS chains (Härtig et al., 1992). The staining was performed on free- floating sections. All incubations were carried out in 24-well plates with 500 microliter per well. After sectioning samples were washed three times using phosphate- buffered saline (PBS; pH 7.4) and then treated for 1 h with a blocking solution containing 5% bovine serum albumin (Sigma) in 0.1 M PBS with 0.5% Triton X-100 (PBST). Streptavidin/Biotin Blocking Kit (VectorLab, USA) was used according to the manufacturers protocol to block endogenous biotin. After that, those sections were quickly rinsed in PBS and incubated overnight at 4 °C using biotinylated Wisteria floribunda agglutinin with final concentration 2 microgram/ml (dilution 1:1000) in 10 mM HEPES and 0.15 M sodium chloride, pH 7.4. Samples were washed three times for 10 min with PBS and incubated for 30 min with AlexaFluor633-conjugated streptavidin (Invitrogen) (dilution 1:500). After that the sections were washed 3 times with PB And pre-treated with 0,3% Triton X-100 for 1 h. Then sections were incubated at blocking solution (5% Normal serum, 1% BSA, 0,3% Triton X-100 in PB) for 1 h and incubated with anti-VGAT IgG (Synaptic Systems) (dilution 1:1000) in PB+ 0,5% Normal serum+ 0,3% Triton X-100 for 48 h at + 4 °C. Samples were washed 3 times for 10 min with PB. Alexa488-conjugated goat anti-rabbit (Thermo-Fisher Scientific) was used as a secondary antibody (dilution 1:200) in phosphate buffer, incubation time 2 h. The sections were mounted on slides, air-dried and coverslipped with ImmunoMount (ThermoScientific).

### 2.4. Confocal microscopy

Brain sections were imaged with laser confocal microscope LSM780 (Carl Zeiss, Jena, Germany), objective lens Plan-Apochromat 63/1.40 Oil DIC M27. Voxel size of 100×100×200 nm was used. PNN-bearing neurons of non-pyramidal morphology were selected within the cortical layer IV.

### 2.5. Image analysis

FIJI (Schindelin et al., 2012) and Imaris (Bitplane) software packages were used for the image analysis. All macros were written in FIJI. The 2D mesh tracing procedure was used as described previously (Arnst et al., 2016). The autothresholding procedure was developed based on the approach described previously (Lipachev et al., 2019). A square area containing a single PNN mesh was subjected to autothresholding using all 17 autothresholding algorithms available in FIJI. As a result, 17 threshold intensity values were obtained and then analyzed together. The intensity range was divided into bins and the final threshold intensity value was calculated as a mean of values falling in the most populated bin and adjacent ones, if their populations were high enough (50% or more of the most populated bin) (Fig. S1). The procedure was first applied to VGAT signal of those meshes oriented parallel to the focal plane. After that the same procedure was applied to the analysis of both WFA and VGAT confocal images of those synapses oriented perpendicularly to the focal plane (transverse section).

By applying the calculated threshold we get the confocal stack masked. We compare the masks of the neighboring layers for matching objects and annotate those as belonging to the same 3D object. The procedure of searching for new elements of the object is repeated through the confocal stack until no new elements are found. This allows us to gradually build up a 3D object. The same z position of a stack is used repeatedly in multiple iterations to search for separate branches of 3D objects with a complex branched geometry.

To calculate the mean width of CS sheath we analyzed profiles of intensities of each pixel of the mesh in the layers below and above the focal plane. The “getPixel” FIJI command was used to find intensities. The intensity values of the traced mesh perimeter were used to set the intensity threshold (30% of the intensity value of the mesh perimeter) for the pixels below and above the initial confocal plane for the detection of the borders of the mesh in the z direction. Then the distances between the upper and lower borders were averaged for all XY positions within the mesh perimeter to get the mesh z-width.

Local intensity maxima for the Z-to-mesh perimeter maps of the CS intensity were calculated with "Find Maxima" command in FIJI.

For 3D analysis of VGAT-positive objects in the focal plane-aligned meshes as well as both WFA-positive and VGAT-positive objects in transverse confocal sections of meshes the algorithm was extended to adequately describe the size and shape changes and branching of the objects between individual confocal planes within a stack.

For the synapse transverse section analysis we designed the following procedure. First, it performs segmentation of the intracellular and extracellular space adjacent to the CS sheath. To select the central line’s joints the FIJI PointPicker plugin was used. That allows us to perform segmentation on the objects with a complex 3D shape that cannot be approximated with a 2D polygon of specific width. After that we calculate coordinates of parallel lines for each segment of the central line that are placed on certain distance from it (Fig. 4). That allows us to segment the object and the space around it into sections.

Statistical analysis is presented for at least 3 independent experiments using one-way ANOVA (Excel, Microsoft). Error bars represent standard error of mean (SEM), symbols * , * * and * ** represent $P <$ 0.05, 0.01, 0.001.

## 3. Results

### 3.1. VGAT distribution in the PNN-synapse complex. 2D analysis

To analyze the morphology of VGAT-positive synaptic boutons we developed an automatic algorithm of the VGAT fluorescence segmentation inside PNN meshes based on the autothresholding function in the FIJI software (Lipachev et al., 2019) (see Methods and Fig. S1). The algorithm allows for unbiased choice of a segmentation threshold for VGAT-positive puncta in a synapse inside a PNN mesh (Fig. S1).

We analyzed 1797 PNN meshes in 38 neurons from 3 mice (Fig. 1A, B) and observed 3 types of the VGAT-positive puncta distribution in PNN meshes on neuronal cell surface (Fig. 1 C-I). A distinct synaptic population had a characteristic morphology with one large cluster of VGAT fluorescence, mean cluster area 0.87 μm$^2$ (STD 0.37 μm$^2$) occupying > 60% of the mesh area (Fig. 1C, D). Another synaptic population had 2–4 smaller VGAT clusters inside each single mesh of PNN (Fig. 1 E, F). Mean VGAT cluster area was 0.22 μm$^2$ (STD 0.12 μm$^2$) for single cluster and 0.7 μm$^2$ (STD 0.17 μm$^2$) for total VGAT cluster area over a single PNN mesh for that population. Finally, a third substantial population had just one small cluster of VGAT per single mesh with a mean cluster area 0.29 μm$^2$ (STD 0.22 μm$^2$) (Fig. 1G, H). A relative occurrence of the 3 types of VGAT distribution is shown in Fig. 1 I. No correlation was observed between the type of VGAT distribution and the PNN mesh area (Data not

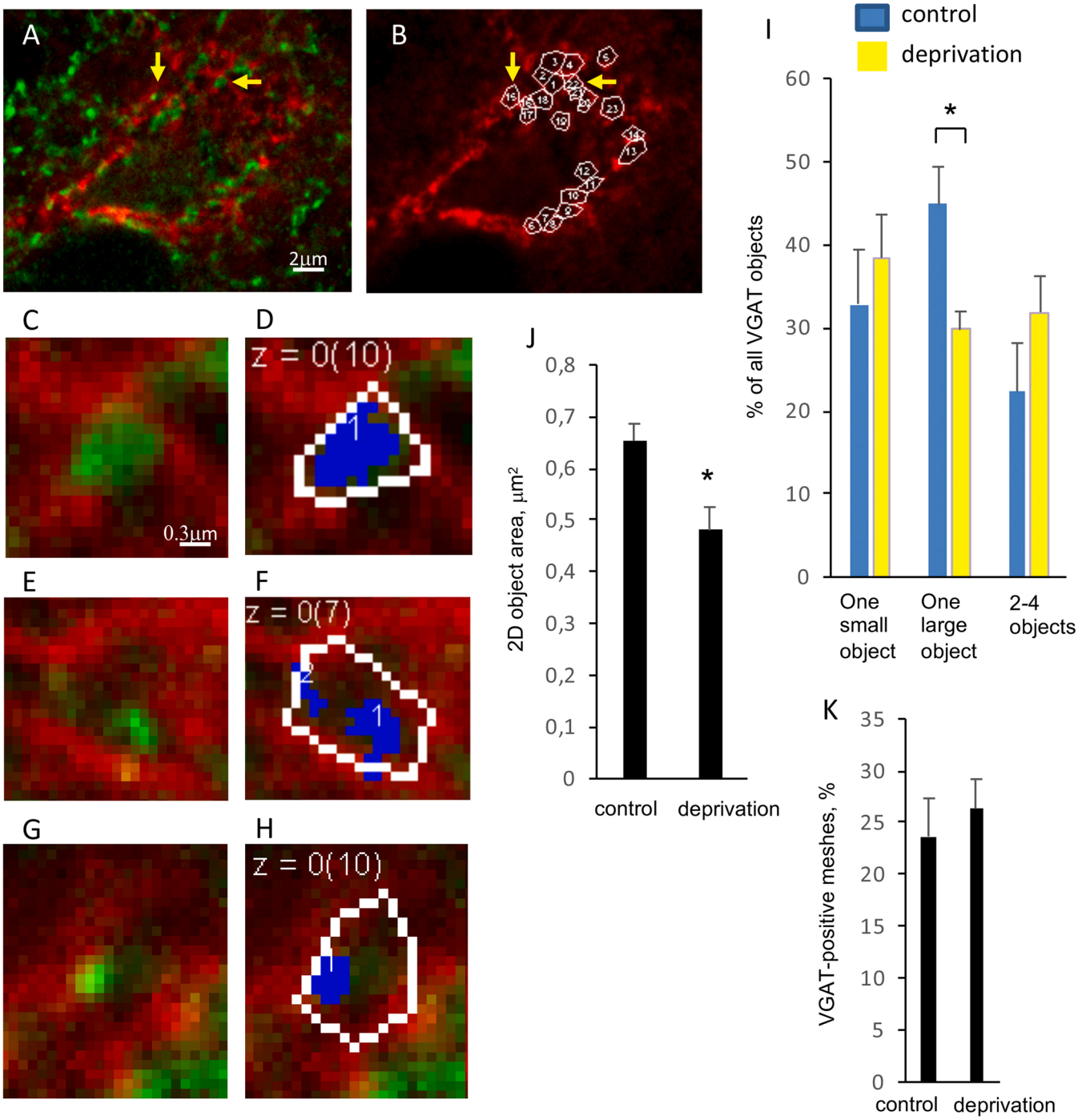


**Fig. 1.** VGAT distribution in the PNN-synapse complex. 2D analysis. A. A PNN-coated neuron in the barrel cortex layer IV. WFA staining for PNN is shownin red, VGAT staining for GABAergic synapses – in green. The arrows in (A, B) mark the PNN meshes 15 and 22 analyzed in further detail in C-D, G-H. B. The same area show in (A) with traced PNN meshes. C. The PNN-synapse complex morphology variant with one large cluster of VGAT. D. The same area as in (C) with the traced PNN mesh (white) and segmented VGAT-positive object (blue). E-F. The morphology variant with 2 (or more) smaller VGAT clusters. G-H. The morphology variant with only 1 small VGAT cluster per mesh. I. Relative occurrence of the PNN-synapse complex morphology variants in the barrel cortex under somatosensory deprivation versus control. J. Average area of VGAT-positive objects within the PNN-synapse complex. K. Occupancy of PNN meshes with VGAT-positive objects under somatosensory deprivation versus control. The scale bar in (A) is valid for (A, B), the scale bar in (C) is valid for (C-H).

shown).

In total 23% of all meshes contained VGAT puncta (Fig. 1K).

### 3.2. Sensory input is required for the proper VGAT distribution within the PNN-synapse complex. 2D analysis

We then asked whether this distribution of the VGAT fluorescence in the PNN-synapse complex is dependent on the sensory input to the developing synaptic network of the brain cortex.

We subjected newborn mice to vibrissae shaving every day during P0-P30 and compared geometry of the GABAergic synapses surrounded with PNN in layer IV of the barrel cortex in deprived versus control littermates. We analyzed 3446 PNN meshes in 76 neurons from 3 independent experiments.

In the 2D analysis we observed significant reduction of occurrence of the morphology variant with single large VGAT cluster under the sensory deprivation as compared to control (Fig. 1I). Consistently, mean area of VGAT-positive objects was reduced in the mice subjected to sensory deprivation (Fig. 1J). About the same portion on meshes contained VGAT-positive objects under sensory deprivation and in control (Fig. 1K).

### 3.3. Sensory input is required for the proper VGAT distribution within the PNN-synapse complex. 3D analysis

We then extended the 2D analysis presented in Fig. 1 to similar 3D procedure on confocal stacks (Fig. 2A-J, L-N). This type of analysis allows to measure 3D geometry of VGAT-positive objects inside PNN meshes (Fig. 2G-J). We observed significant reduction of occurrence of the morphology variant with single large 3D cluster of VGAT under the sensory deprivation as compared to control (Fig. 2L) supporting the results of 2D analysis (Fig. 1I). Furthermore, mean volume of VGAT-positive 3D objects was reduced in the mice subjected to sensory deprivation (Fig. 2M).

### 3.4. Sensory deprivation affects the relative spatial distribution of VGAT versus PNN

We further expanded the 3D analysis of the PNN+synapse complex geometry by analyzing the choldroitin sulphates (CS) staining intensity distribution along the Z axis and the mesh perimeter (Fig. 2K). That type of analysis allowed us to measure relative distribution of the VGAT and CS signals along the Z coordinate (Fig. 2G, J, K). Fig. 2O demonstrates average values of root mean square deviation (RMSD) for the Z position of the highest mean intensity of the CS signal along the mesh perimeter to the Z position of - 1) the area maximum, 2) the mean intensity maximum, 3) the median - of the VGAT signal 3D distribution under somatosensory deprivation versus control.

The intensity maximum of CS within the mesh perimeter and the area maximum of VGAT within the synaptic terminal are shifted relative to each other along the Z coordinate under somatosensory deprivation as compared to control (Fig. 2O).

### 3.5. Sensory input is required for the proper morphogenesis of the PNN meshes

To address the effect of sensory deprivation on the PNN geometry we first analyzed the mesh area in the PNNs from animals with shaved whiskers versus controls. We could see no significant difference in the shape, area and the chondroitin sulfate staining distribution between the two groups (Data not shown). We then analyzed 3-dimensional distribution of the CS staining intensity along the mesh perimeter (Fig. 3). We calculate the mean CS intensity along the mesh perimeter for each confocal plane and use 10% of the highest value as the segmentation threshold along the Z axis to define the upper and lower border of the mesh (shown in green in Fig. 3E, F). We demonstrate that the mean Z-width (or “thickness”) of PNN meshes decreases upon somatosensory deprivation (Fig. 3E, F, I).

We further demonstrate that RMSD between the Z position of the highest mean intensity and z positions of local intensity maxima decreased significantly under somatosensory deprivation (Fig. 3J, K), i.e., the meshes become more flattened if the developing brain cortex lacks the sensory input.

As both the VGAT-positive volume and the PNN mesh thickness were affected by sensory deprivation (Fig. 2M, 3E, F, I) we then asked the question whether those two parameters correlate with each other. We observed no pronounced correlation between the VGAT volume and the Z-width or between the VGAT volume and the RMSD of intensity maxima (correlation coefficients $r = 0.148$ and 0.271, respectively).

### 3.6. Sensory input is required for the proper morphogenesis of the PNN-synapse complex. The synapse transverse section analysis

To validate our findings of the PNN mesh flattening and reduction of the VGAT cluster volume caused by sensory deprivation we took an alternative approach to the PNN 3D geometry quantification by analyzing transverse sections of the PNN-covered neuronal cell surface (Fig. 4). As XY resolution of confocal microscopy is remarkably higher than Z resolution, so one advantage of this approach is that a side projection of the mesh is oriented in the confocal plane (XY plane) rather than in Z dimension resulting in higher spatial resolution of the image data.

We performed 3D analysis analogous to what we did on meshes oriented along the confocal plane (Fig. 2J, M) and confirmed the reduction of the mean VGAT cluster volume under somatosensory deprivation as compared to control (Fig. 4A-E, K).

We then performed segmentation of the intracellular and extracellular space adjacent to the CS sheath (Fig. 4F-J) and demonstrated that the width (“thickness”) of the CS sheath surrounding VGAT-positive synapses is reduced under somatosensory deprivation as compared to control (Fig. 4I).

## 4. Discussion

The effect of the sensory input on neuronal plasticity has been widely studied following the classical work of Wiesel and Hubel on monocular deprivation (Wiesel and Hubel, 1965; Fagiolini et al., 1994, Berardi et al., 2000). Developmental increase of the activity of cortical inhibitory circuits has been shown to contribute to the closure of the critical period of cortical synaptic network plasticity (Hensch et al., 1998; Huang et al., 1999; Kirkwood et al., 1994).

The experimental evidence on physiological and pathological roles of PNN has been accumulating rapidly over the last decade (Bitanihirwe et al., 2016; Pantazopoulos and Berretta, 2016). This evidence of functional importance raises the question of the structural mechanism for the PNN function. Nevertheless, quantitative structural studies of the PNN fine structure remained absent until recently (Arnst et al., 2016; Dzyubenko et al., 2018; Sigal et al., 2019; Kaushik et al., 2020).

A functional hallmark of the brain cortex postnatal development from the immature to the mature state is a drastic decrease of neuronal plasticity and perineuronal nets were systematically shown to play a major role in that developmental switch (Pizzorusso et al., 2002). Developmental changes in the CSPG expression were previously studied in particular detail in the brain visual cortex. Distinct CSPG epitopes both in the CS moiety and in the protein core exhibit activity-dependent expression in visual cortex at the closure of critical period in the cat model of dark rearing (Lander et al., 1997). Similar reduction of CSPG epitopes was reported in cat lateral geniculate nucleus upon dark rearing (Sur et al., 1988; Guimaraes et al., 1990; Kind et al., 1995).

In the layer IV of the barrel cortex perineuronal nets are formed at the end of the critical period of plasticity (Köppe et al., 1997). Consistently, a significant portion of the neuronal plasticity processes round up

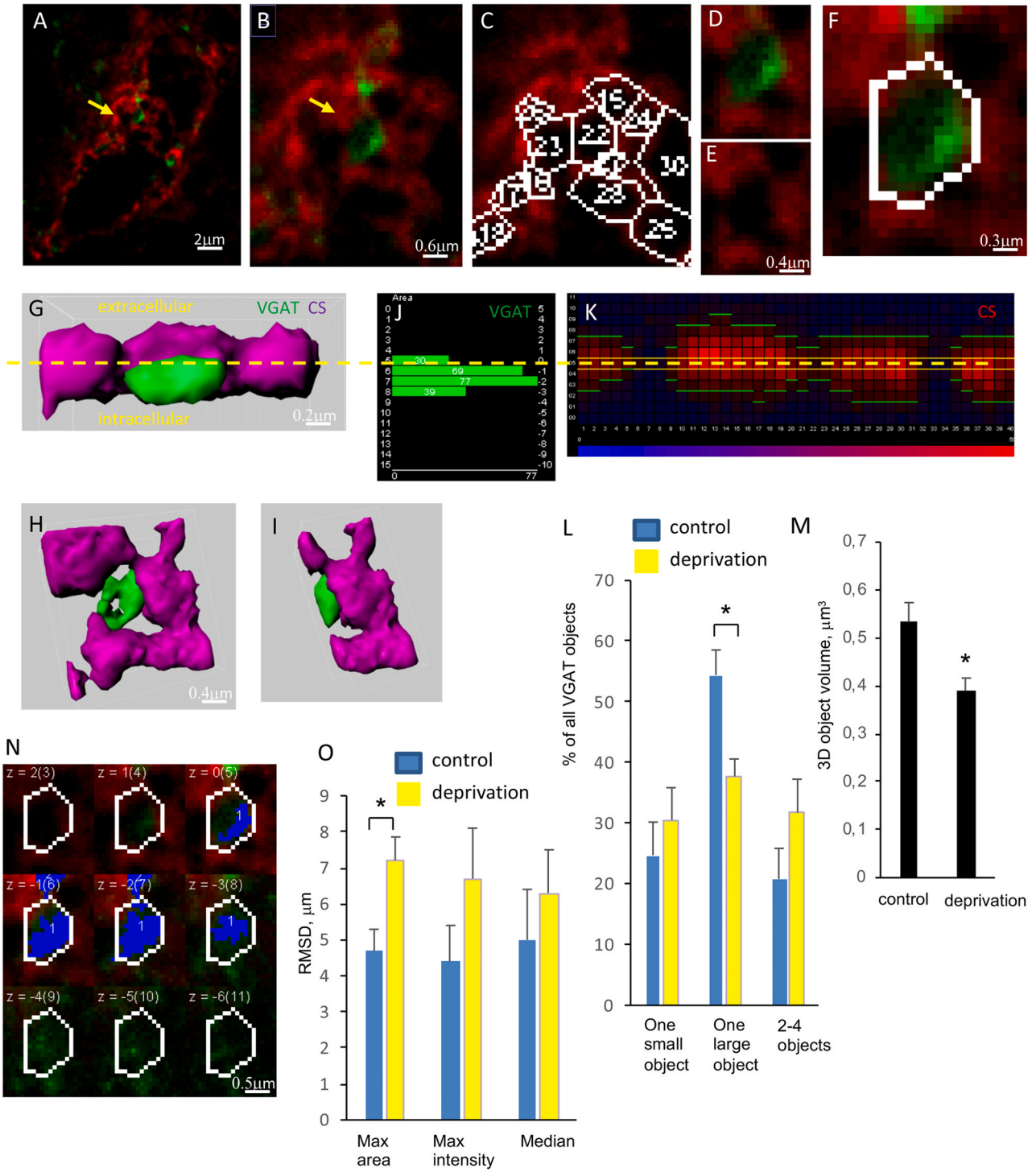


**Fig. 2.** Sensory input is required for the proper VGAT distribution in the PNN-synapse complex. A. A PNN-coated neuron in the barrel cortex layer IV. WFA staining for PNN is shown in red, VGAT staining for GABAergic synapses – in green. The arrow marks the synapse analyzed in further detail in B-I, N. B. An enlarged cell surface area of the same neuron show in (A). C. The same area as in (B) with traced meshes. D-F. Enlarged mesh 22 from the map shown in (C). G-I. 3D reconstruction of the VGAT (green) and WFA (purple) fluorescence from the confocal stack for the PNN mesh shown in (F). G. *In silico* transversal cut of the synaptic terminal and the surrounding PNN. H. The focal plane view of the mesh. I. The same *in silico* transversal cut as in (H), focal plane view. J. The Z distribution of the segmented VGAT-positive object area for the synaptic terminal shown in (F). K. The Z distribution of the WFA fluorescence intensity (color-coded blue-red, the color code given in the bottom of the panel) along the perimeter of the mesh. The perimeter is shown in white in (F). The Z axis of the confocal stack is aligned for (G, J, K). The Z plane with the maximal WFA signal intensity along the mesh perimeter is chosen as Z = 0. L. Relative abundance of the morphology variants of VGAT-positive objects surrounded by the perineuronal net under somatosensory deprivation and in control. M. Average volume of VGAT-positive objects surrounded by the perineuronal net. N. Segmentation of VGAT-positive objects in sequential confocal images within a confocal stack for the mesh shown in (F). O. Root mean square deviation between the Z = 0 (the plane with the highest WFA intensity along the mesh perimeter) and the Z position corresponding to the maximal area, maximal intensity or the median Z position of the VGAT-positive 3D objects inside the PNN mesh.

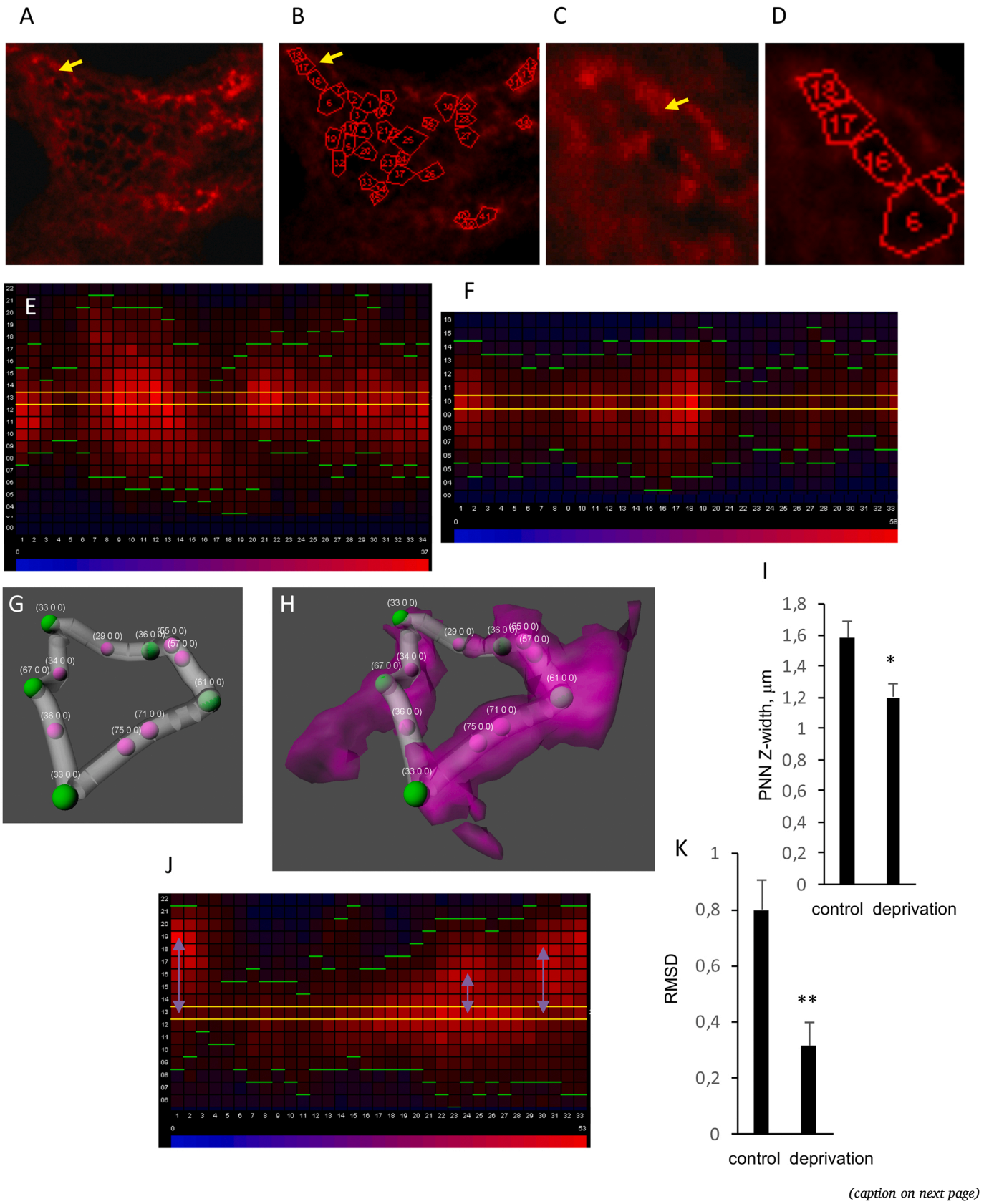


*(caption on next page)*

**Fig. 3.** Sensory input is required for the proper morphogenesis of the PNN meshes. A. A PNN-coated neuron in the barrel cortex layer IV, stained with WFA. The arrow in (A-C) marks mesh 17 analyzed in further detail in B-E, G-H. B. The same image as in (A) with traced PNN meshes. C-D. An enlarged cell surface area with the mesh 17 of the same neuron as in (A). E. The Z distribution of the WFA fluorescence intensity (color-coded blue-red, the color code given in the bottom of the panel) along the perimeter of the mesh 17. The green borders depict 90% drop of the fluorescence intensity as compared to the Z layer with the highest intensity (shown in yellow).The perimeter is shown in red in (D). F. The Z distribution of the WFA fluorescence intensity along the perimeter for a mesh of a barrel cortex layer IV neuron following somatosensory deprivation. G. The filament autodepth 3D reconstruction of the mesh 17 shown in (C-E). The mesh vertices are shown in green, the middle pixels of edges are shown in magenta, corresponding values of fluorescence intensity are given in brackets. H. The same filament reconstruction as in (G) supplemented with the 3D surface reconstruction of the WFA staining fluorescence intensity. I. Average values for the Z width of the PNN meshes under somatosensory deprivation and in control based on the 90% cut-off for the WFA staining intensity. J. The Z distribution of the WFA fluorescence intensity along the perimeter for a mesh in a control mouse. Arrows show the distance between the Z layer with the highest WFA staining intensity and local intensity maxima within the map. K. Average values of RMSD between the Z layer with the highest WFA staining intensity and local intensity maxima of the Z-perimeter intensity maps under the somatosensory deprivation and in control.

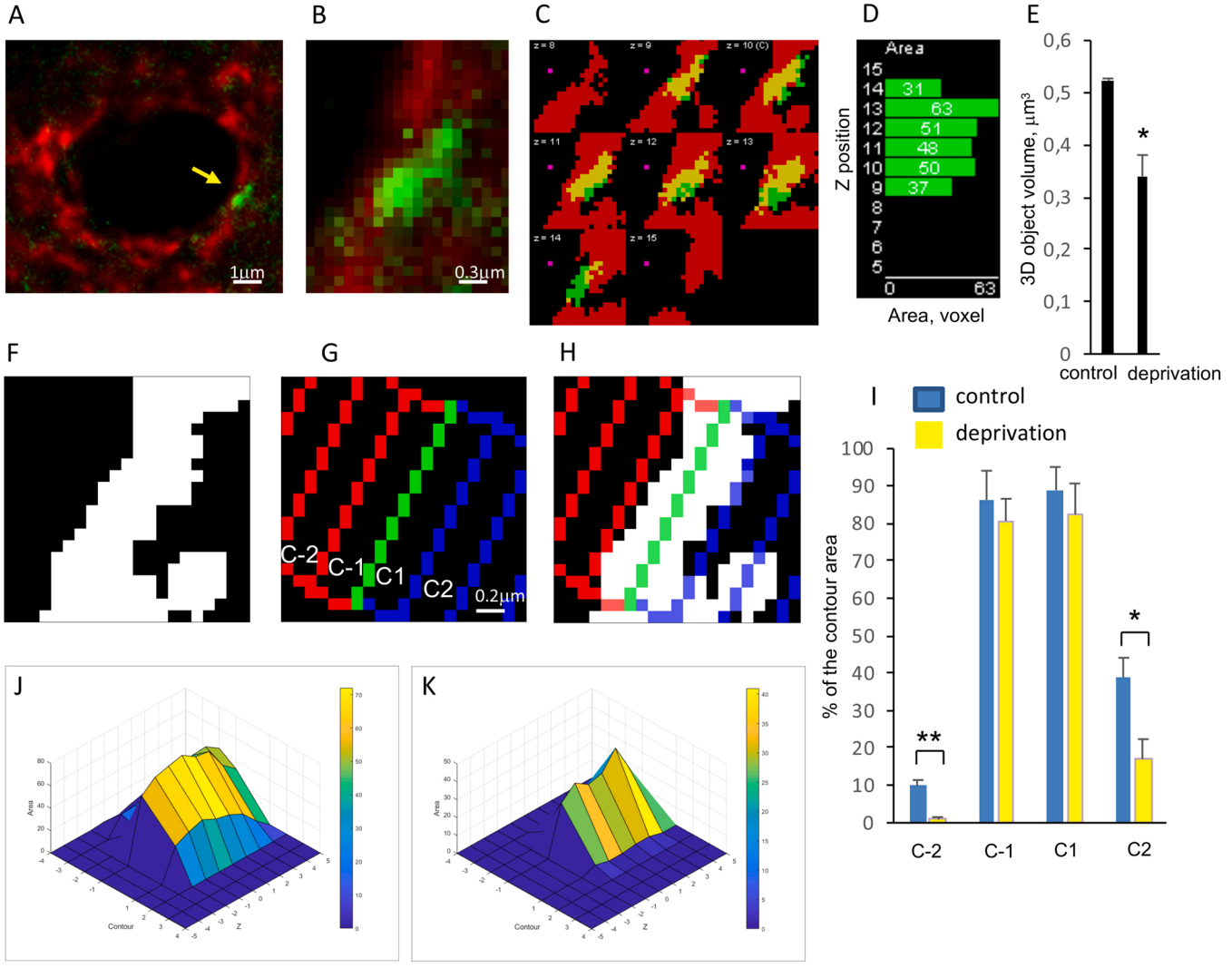


**Fig. 4.** The synapse transverse section analysis. A. A PNN-coated neuron in the barrel cortex layer IV. The arrow marks a transverse confocal section of the PNN-coated cell surface (red for WFA) with a GABAergic synapse (green for VGAT) analyzed in further detail in B-D,F-H, J-K. B. An enlarged cell surface area of the same neuron shown in (A) with the synapse surrounded by PNN. C. Segmentation of VGAT-positive (shown in green) and WFA-positive (shown in red) objects in sequential confocal images within a confocal stack for the synapse shown in (B). The overlay of the VGAT- and WFA-positive object masks is shown in yellow. The magenta dot marks the intracellular side. D. The Z distribution of the segmented VGAT-positive object area for the synaptic terminal shown in (B). E. Average volume of VGAT-positive objects surrounded by the perineuronal net as a result of the transverse synapse section analysis for somatosensory deprivation versus controls. F. The WFA-positive object mask for the synapse shown in (B). G-H. Segmentation of the image in (F) into contours based on the distance from the central line of the PNN layer (shown in green) towards the extracellular (blue contours) and intracellular (red contours) space. I. Quantification of the thickness of the cell surface PNN layer presented as a contour area occupancy by the WFA-positive objects. Comparison for sensory deprivation versus control. J-K. The object area distribution for the WFA-positive (J) and VGAT-positive (K) objects in the Z-contour coordinate space for the synapse shown in (B).

by the end of the first postnatal month in the mouse barrel cortex (Fox, 2002; Glazewski and Fox, 1996).

We previously hypothesized that the spatial structure of the perineuronal net surrounding a synaptic bouton should play an important role in the synapse physiology (Arnst et al., 2016) based on the experimental data demonstrating that CSPG bind extracellular $Ca^{2+}$ and

a range of signaling ligands including pleiotrophin, VEGF, GDNF (Paveliev et al., 2016; Rauvala et al., 2017; Nandini et al., 2004).

We previously developed a mesh-tracing method for quantification of the mesh geometry and molecular epitope distribution along the mesh perimeter (Arnst et al., 2016). The initial aim of the present study was to study the synaptic terminal microstructure inside the mesh under the control and somatosensory deprivation conditions. We also wanted to search for correlation between the synaptic terminal and the surrounding PNN mesh geometry parameters in order to understand the integral architecture of the synapse + PNN complex as a functional unit.

For that purpose we developed a "synthetic" autothresholding algorithm to measure parameters of the VGAT GABA transporter spatial distribution within a synaptic terminal surrounded by a PNN mesh (Fig. 1, S1). That approach is an extension of our previous procedure using 16 different autothresholding algorithms provided by FIJI (Lipachev et al., 2019). With this method we are aiming at an automatic and unbiased image segmentation procedure retrieving as accurate structural information from the brain tissue confocal images as possible.

Quantitative distribution of VGAT within the GABAergic synaptic terminals remains poorly studied. In their pioneering study of the cerebellar synapse ultrastructure Chaundhry and co-authors demonstrated that VGAT co-localized with synaptic vesicles and was absent from other compartments of a synaptic terminal (Chaudhry et al., 1998).

These data suggest that the VGAT signal observed in our study corresponds to the distribution of vesicles with the neurotransmitter next to the GABAergic synapse active zones. Our observation on the reduction of the VGAT immunofluorescence cluster size resulting from the somatosensory deprivation (Figs. 1, 2, 4) leads to the conclusion that the sensory input is essential for the proper synapse geometry formation during development, more specifically – during the critical period of the mouse brain cortex synaptic plasticity within the first postnatal month.

Whisker trimming in neonatal mice causes reduction in the aggrecan mRNA expression and Cat-315 immunoreactivity in the barrel cortex (McRae et al., 2007). Taken together the results by McRae and co-authors (McRae et al., 2007) and our results presented here demonstrate that somatosensory deprivation causes changes both in the molecular composition and 3D structure of the perineuronal net (Fig. 3) and in the spatial structure of the synaptic terminals embedded in the PNN (Fig. 2). Possible causal connections between those effects remain to be investigated.

We previously analyzed the 3D spatial structure of PNN using the autodepth filament tool of the Imaris software (Arnst et al., 2016). Here we expand the analysis repertoire by measuring the CS epitope distribution along the mesh perimeter also in the Z direction (Fig. 2K, 3). That gives a quantitative estimate of the mesh width and curvature along the Z axis. Moreover, that approach allows us calculating a Z position with the highest average intensity of the CS signal to be used as a "0 coordinate" of the mesh geometry for the quantification of relative positions of VGAT-positive objects within the synapse + PNN complex (Fig. 2G, J, K, O).

The 2D area and 3D volume of VGAT-positive objects (Fig. 1C-J, Fig. 2J, L-N) could be viewed as characteristics of the synaptic vesicle pool size. That is a crucial parameter for the synaptic function and thus our quantitative studies on the VGAT-positive object microstructure and distribution should shed light on the structural and functional connection between the synapse and the surrounding PNN.

The approach presented here for quantitative structural studies and the results on the synaptic terminal + PNN complex 3D structure contribute to understanding coordination between the ECM and synaptic network and the molecular physiological mechanisms connecting these two brain components into an integral structural and functional unit.

## 5. Conclusion

To summarize, our data demonstrate that the fine microstructure of the cortical GABAergic synaptic terminals and surrounding PNN meshes develops postnatally under the influence of sensory input so that withdrawal of the input leads to malformation of particular structural features of the synapse + PNN complex.

## Funding

Sample preparation was funded by Russian Foundation for Basic Research (project number 20-315-90074). The work was performed according to the Russian Government Program of Competitive Growth of Kazan Federal University. This paper has been supported by the Kazan Federal University Strategic Academic Leadership Program (PRIORITY-2030).

## Ethical approval

BalbC mice were used according to regulations of the ethics committee of Kazan Federal University.

## CRediT authorship contribution statement

**Nikita Lipachev:** Conceptualization, Methodology, Software, Validation, Formal analysis, Investigation, Data curation, Writing – review & editing, Visualization, Funding acquisition. **Anastasia Melnikova:** Methodology, Validation, Investigation, Data curation, Visualization, Funding acquisition. **Svetlana Fedosimova:** Methodology, Investigation, Resources, Supervision. **Nikita Arnst:** Methodology, Validation, Investigation. **Anastasia Kochneva:** Validation, Data curation, Visualization. **Nurislam Shaikhutdinov:** Investigation. **Anastasia Dvoeglazova:** Data curation, Visualization. **Angelina Titova:** Investigation, Resources, Supervision. **Mikhail Mavlikeev:** Investigation, Resources, Supervision, Project administration. **Albert Aganov:** Resources, Supervision, Project administration, Funding acquisition. **Yuri Osin:** Methodology, Resources, Supervision. **Andrei Kiyasov:** Resources, Supervision, Project administration. **Mikhail Paveliev:** Conceptualization, Methodology, Software, Validation, Formal analysis, Resources, Data curation, Writing – original draft, Writing – review & editing, Visualization, Supervision, Project administration, Funding acquisition.

## Conflict of interest

The authors of this publication declare no competing or financial interests.

## Appendix A. Supporting information

Supplementary data associated with this article can be found in the online version at doi:10.1016/j.neures.2022.06.005.

## References

Arnst, N., Kuznetsova, S., Lipachev, N., Shaikhutdinov, N., Melnikova, A., Mavlikeev, M., Uvarov, P., Baltina, T.V., Rauvala, H., Osin, Yu. N., Kiyasov, A.P., Paveliev, M., 2016. Spatial patterns and cell surface clusters in perineuronal nets. Brain Res. 1648 (Part A), 214–223. https://doi.org/10.1016/j.brainres.2016.07.020.

Berardi, N., Pizzorusso, T., Maffei, L., 2000. Critical periods during sensory development. Curr. Opin. Neurobiol. 10, 138–145.

Bitanihirwe, B.K., Mauney, S.A., Woo, T.U., 2016. Weaving a net of neurobiological mechanisms in Schizophrenia and unraveling the underlying pathophysiology. Biol. Psychiatry 80 (8), 589–598. https://doi.org/10.1016/j.biopsych.2016.03.1047.

Brückner, G., Kacza, J., Grosche, J., 2004. Perineuronal nets characterized by vital labelling, confocal and electron microscopy in organotypic slice cultures of rat parietal cortex and hippocampus. J. Mol. Histol. 35, 115–122. https://doi.org/10.1023/B:HIJO.0000023374.22298.50.

Carulli, D., Pizzorusso, T., Kwok, J.C.F., Putignano, E., Poli, A., Forostyak, S., Andrews, M.R., Deepa, S.S., Glant, T.T., Fawcett, J.W., 2010. Animals lacking link protein have attenuated perineuronal nets and persistent plasticity. Brain 133, 2331–2347. https://doi.org/10.1093/brain/awq145.

Chaudhry, F.A., Reimer, R.J., Bellocchio, E.E., Danbolt, N.C., Osen, K.K., Edwards, R.H., Storm-Mathisen, J., 1998. The vesicular GABA transporter, VGAT, localizes to

synaptic vesicles in sets of glycinergic as well as GABAergic neurons. J Neurosci. 18 (23), 9733–9750. https://doi.org/10.1523/JNEUROSCI.18-23-09733.1998.

Dzyubenko, E., Gottschling, C., Faissner, A., 2016. Neuron-glia interactions in neural plasticity: contributions of neural extracellular matrix and perineuronal nets. Neural Plast., 5214961 https://doi.org/10.1155/2016/5214961.

Dzyubenko, E., Manrique-Castano, D., Kleinschnitz, C., Faissner, A., Hermann, D.M., 2018. Topological remodeling of cortical perineuronal nets in focal cerebral ischemia and mild hypoperfusion. Matrix Biol. 74, 121–132. https://doi.org/10.1016/j.matbio.2018.08.001.

Fagiolini, M., Pizzorusso, T., Berardi, N., Domenici, L., Maffei, L., 1994. Functional postnatal development of the rat primary visual cortex and the role of visual experience: dark rearing and monocular deprivation. Vis. Res. 34, 709–720.

Fawcett, J.W., Oohashi, T., Pizzorusso, T., 2019. The roles of perineuronal nets and the perinodal extracellular matrix in neuronal function. Nat. Rev. Neurosci. 20 (8), 451–465. https://doi.org/10.1038/s41583-019-0196-3.

Ferrer-Ferrer, M., Dityatev, A., 2018. Shaping synapses by the neural extracellular matrix. Front Neuroanat. 15, 12–40. https://doi.org/10.3389/fnana.2018.00040.

Fox, K., 2002. Anatomical pathways and molecular mechanisms for plasticity in the barrel cortex. Neuroscience 111, 799–814.

Glazewski, S., Fox, K., 1996. Time course of experience-dependent synaptic potentiation and depression in barrel cortex of adolescent rats. J. Neurophysiol. 75 (4), 1714–1729. https://doi.org/10.1152/jn.1996.75.4.1714.

Guimaraes, A., Zaremba, S., Hockfield, S., 1990. Molecular and morphological changes in the cat lateral geniculate nucleus and visual cortex induced by visual deprivation are revealed by monoclonal antibodies Cat-304 and Cat-301. J. Neurosci. 10, 3014–3024.

Härtig, W., Brauer, K., Brückner, G., 1992. Wisteria floribunda agglutinin-labelled nets surround parvalbumin-containing neurons. Neuroreport 3, 869–872. https://doi.org/10.1097/00001756-199210000-00012.

Hensch, T.K., Fagiolini, M., Mataga, N., Stryker, M.P., Baekkeskov, S., Kash, S.F., 1998. Local GABA circuit control of experience-dependent plasticity in developing visual cortex. Science 282, 1504–1508.

Huang, Z.J., Kirkwood, A., Pizzorusso, T., Porciatti, V., Morales, B., Bear, M.F., Maffei, L., Tonegawa, S., 1999. BDNF regulates the maturation of inhibition and the critical period of plasticity in mouse visual cortex. Cell 98, 739–755.

Kaushik, R., Lipachev, N., Matuszko, G., Kochneva, A., Dvoeglazova, A., Becker, A., Paveliev, M., Dityatev, A., 2020. Fine structure analysis of perineuronal nets in the ketamine model of schizophrenia. Eur. J. Neurosci. 2020 (Jun 8) https://doi.org/10.1111/ejn.14853.

Kind, P.C., Beaver, C.J., Mitchell, D.E., 1995. Effects of early periods of monocular deprivation and reverse lid suture on the development of Cat-301 immunoreactivity in the dorsal lateral geniculate nucleus of the cat. J. Comp. Neurol. 359, 523–536.

Kirkwood, A., Lee, H.K., Bear, M.F., 1994. Co-regulation of long-term potentiation and experience-dependent synaptic plasticity in visual cortex by age and experience. Nature 375, 328–331.

Köppe, G., Brückner, G., Brauer, K., Härtig, W., Bigl, V., 1997. Developmental patterns of proteoglycan-containing extracellular matrix in perineuronal nets and neuropil of the postnatal rat brain. Cell Tissue Res. 288 (1), 33–41. https://doi.org/10.1007/s004410050790.

Lander, C., Kind, P., Maleski, M., Hockfield, S., 1997. A family of activity-dependent neuronal cell-surface chondroitin sulfate proteoglycans in cat visual cortex. J. Neurosci. 17, 1928–1939.

Lipachev, N., Arnst, N., Melnikova, A., Jäälinoja, H., Kochneva, A., Zhigalov, A., Kulesskaya, N., Aganov, A.V., Mavlikeev, M., Rauvala, H., Kiyasov, A.P., Paveliev, M., 2019. Quantitative changes in perineuronal nets in development and posttraumatic condition. J. Mol. Histol. 50 (3), 203–216. https://doi.org/10.1007/s10735-019-09818-y.

McRae, P.A., Rocco, M.M., Kelly, G., Brumberg, J.C., Matthews, R.T., 2007. Sensory deprivation alters aggrecan and perineuronal net expression in the mouse barrel cortex. J. Neurosci. 27, 5405–5413.

Miyata, S., Kitagawa, H., 2017. Formation and remodeling of the brain extracellular matrix in neural plasticity: roles of chondroitin sulfate and hyaluronan. Biochim Biophys. Acta Gen. Subj. 1861 (10), 2420–2434. https://doi.org/10.1016/j.bbagen.2017.06.010.

Nandini, C.D., Mikami, T., Ohta, M., Itoh, N., Akiyama-Nambu, F., Sugahara, K., 2004. Structural and functional characterization of oversulfated chondroitin sulfate/dermatan sulfate hybrid chains from the notochord of hagfish. Neuritogenic and binding activities for growth factors and neurotrophic factors. J. Biol. Chem. 279, 50799–50809. https://doi.org/10.1074/jbc.M404746200.

Nowicka, D., Soulsby, S., Skangiel-Kramska, J., Glazewski, S., 2009. Parvalbumin-containing neurons, perineuronal nets and experience-dependent plasticity in murine barrel cortex. Eur. J. Neurosci. 30 (11), 2053–2063. https://doi.org/10.1111/j.1460-9568.2009.06996.x. Epub 2009 Nov 25.

Pantazopoulos, H., Berretta, S., 2016. In sickness and in health: perineuronal nets and synaptic plasticity in psychiatric disorders. Neural Plast. 2016, 9847696 https://doi.org/10.1155/2016/9847696.

Paveliev, M., Fenrich, K.K., Kislin, M., Kuja-Panula, J., Kulesskiy, E., Varjosalo, M., Kajander, T., Mugantseva, E., Ahonen-Bishopp, A., Khiroug, L., Kulesskaya, N., Rougon, G., Rauvala, H., 2016. HB-GAM (pleiotrophin) reverses inhibition of neural regeneration by the CNS extracellular matrix. Sci. Rep. 6 (2016), 33916 https://doi.org/10.1038/srep33916.

Pizzorusso, T., Medini, P., Berardi, N., Chierzi, S., Fawcett, J.W., Maffei, L., 2002. Reactivation of ocular dominance plasticity in the adult visual cortex. Science 298, 1248–1251.

Rauvala, H., Paveliev, M., Kuja-Panula, J., Kulesskaya, N., 2017. Inhibition and enhancement of neural regeneration by chondroitin sulfate proteoglycans. Neuron Regen. Res. 12, 687–691. https://doi.org/10.4103/1673-5374.206630.

Schindelin, J., Arganda-Carreras, I., Frise, E., Kaynig, V., Longair, M., Pietzsch, T., Preibisch, S., Rueden, C., Saalfeld, S., Schmid, B., Tinevez, J.Y., White, D.J., Hartenstein, V., Eliceiri, K., Tomancak, P., Cardona, A., 2012. Fiji: an open-source platform for biological-image analysis. Nat. Methods 9, 676–682. https://doi.org/10.1038/nmeth.2019.

Sigal, Y.M., Bae, H., Bogart, L.J., Hensch, T.K., Zhuang, X., 2019. Structural maturation of cortical perineuronal nets and their perforating synapses revealed by superresolution imaging. Proc. Natl. Acad. Sci. USA 116 (14), 7071–7076. https://doi.org/10.1073/pnas.1817222116.

Sorg, B.A., Berretta, S., Blacktop, J.M., Fawcett, J.W., Kitagawa, H., Kwok, J.C., Miquel, M.J., 2016. Casting a wide net: role of perineuronal nets in neural plasticity. Neurosci 36 (45), 11459–11468. https://doi.org/10.1523/JNEUROSCI.2351-16.2016.

Sur, M., Frost, D.O., Hockfield, S., 1988. Expression of a surface-associated antigen on Y-cells in the cat lateral geniculate nucleus is regulated by visual experience. J. Neurosci. 8, 874–882.

Wiesel, T.N., Hubel, D.H., 1965. Extent of recovery from the effects of visual deprivation in kittens. J Neurophysiol. 28 (6), 1060–1072. https://doi.org/10.1152/jn.1965.28.6.1060.